Int. J. Appl. Comput. Math (2024) 10:95
https://doi.org/10.1007/s40819-024-01734-4

ORIGINAL PAPER

Numerical Analysis of MHD Hybrid Nanofluid Flow a Porous Stretching Sheet with Thermal Radiation

Shiva Rao[1] · **P. N. Deka**[2]

Accepted: 19 March 2024

Abstract
The current investigation considers the two-dimensional time independent MHD flow and heat transfer of a water-based hybrid nanofluid induced by a stretching sheet of porous medium with first order boundary slip conditions. The Effects of thermal radiation, viscous dissipation, and Joule heating are taken into consideration. For investigation, hybrid nanoparticles of silver (Ag) and alumina (Al_2O_3) are considered along with water (H_2O) as base fluid. Following a suitable similarity transformation, the governing equations are reconstructed as a set of non-linear ordinary differential equations. The equations are solved using the Keller-box numerical technique. The influence of different parameters on the velocity profile and temperature profile are illustrated graphically, whereas its impact on skin-friction coefficient and local Nusselt number are tabulated. From this study, it is concluded that the thermal boundary layer thickness increases with an increase in the radiation and magnetic parameter. Furthermore, it is observed that the speed of the hybrid nanofluid can be controlled by applying a magnetic field, porous media, and enhancing the volume fraction of the nanoparticles. It is found that better results are shown by the use of hybrid nanofluid ($Ag - Al_2O_3/water$) compared to the nanofluids with single nanoparticles ($Ag/water$). An excellent comparison with previously published works is presented in the current article.

Keywords Thermal radiation · Viscous dissipation · Nanofluid · Joule heating · Stretching sheet · Slip effect

List of symbols

c	Constant
x, y	Cartesian coordinates along the surface and normal to it, respectively (m)
u, v	Velocity component along x-axis and y-axis respectively (m s^{-1})

✉ Shiva Rao
shivarao374@gmail.com

P. N. Deka
pndeka@dibru.ac.in

[1] Department of Mathematics, Bapujee College, Barpeta 781307, India

[2] Department of Mathematics, Dibrugarh University, Dibrugarh 786004, India

Published online: 09 April 2024

T	Temperature (K)
B_o	Magnetic field (T)
k_o	Porous term (m^2)
C_p	Specific heat at constant pressure (J kg^{-1} K^{-1})
q_r	Radiative heat flux
k^*	Mean absorption co-efficient
M	Magnetic parameter
Re_x	Reynold number
K_p	Permeability parameter
Ec	Eckert number
Pr	Prandtl number
R	Radiation parameter
N	Velocity slip factor
D	Thermal slip factor
f	Dimensionless stream function
q_w	Surface heat flux
Cf_x	Skin-friction coefficient
Nu_x	Nusselt number

Greek Symbols

ν	Kinematic viscosity (m^2 s^{-1})
μ	Dynamic viscosity (kg m^{-1} s^{-1})
σ	Electrically conductivity (S m^{-1})
ρ	Density (kg m^{-3})
κ	Thermal conductivity of the nanofluid
α	Thermal diffusivity (m^2 s^{-1})
ϕ_1	Volume fraction of Ag nanoparticle
ϕ_2	Volume fraction of Al_2O_3 nanoparticle
σ^*	Stefan-Boltzmann coefficient
θ	Dimensional temperature
λ	Velocity slip parameter
δ	Thermal slip parameter

Superscript

$'$	Derivative with respect to η

Subscript

w	At wall
∞	At free stream region
hnf	For hybrid nanofluid
nf	For nanofluid with single nanoparticle
f	For base fluid

$s1$ For Ag nanoparticle
$s2$ For Al_2O_3 nanoparticle

Introduction

Due to its wide range of applications in biomedicine, heat exchangers, cooling of electrical devices, double-pane windows, food, transportation, etc., nanofluids has become a more widespread area of research for scientists in recent times. To enhance the thermal conductivity of base fluids such as ethylene glycol, water, kerosene, and motor oils, it is necessary to add nanoparticles such as graphene, silica, silver, gold, copper, alumina, carbon nanotubes, etc. The diameter of such nanoparticles may vary anywhere from 1 to 100 nm. It was first observed by Choi [1] that the thermal conductivity of the base fluid could be enhanced by nanoparticles, improving the fluid's heat transfer rate. Later, the factors influencing the thermal conductivity of nanofluids were investigated by Buongiorno [2], who reported that Brownian motion and thermophoresis effects increase the thermal conductivity of the nanofluid. As a consequence of this revelation, Buongiorno's model was used on the boundary layer stream by Nield and Kuznetsov [3]. The steady flow of nanofluid on a stretching sheet was first explored by Khan and Pop [4]. The heat transfer characteristics of nanofluid flow were investigated by Makinde and Aziz [5] using convective boundary conditions.

A new type of fluid called a hybrid nanofluid, is finding widespread technological usage due to its excellent thermophysical properties. The advanced fluid, composed by adding two or more nanoparticles in a base fluid, is referred to as hybrid nanofluids. Such kinds of nanofluids have more superior properties than conventional nanofluids. An individual substance may never possess all of the needed traits; hence, the substance may be missing or deficient in some properties. Customizable hybrid nanoparticles can process important information more effectively than other nanofluids. Nanofluids are ordinarily outperformed by hybrid nanofluids in a variety of heat transfer applications, making them ideal for use in industries as diverse as refrigeration, electronics cooling, drug reduction, generator cooling, machining coolant, cooling for nuclear systems, cooling for transformers, biomedicine, and many more. A detailed procedure for creating hybrid nanofluids, including their benefits and drawbacks, was been suggested by Sundar [6]. The unsteady flow of a hybrid nanofluid made by adding Cu nanoparticles in Al_2O_3/water nanofluid due to a stretching/shrinking sheet has been studied by Waini et al. [7]. The effect of thermal radiation, chemical reaction, suction, and slip condition for the heat and mass transfer of an unsteady MHD flow over a stretching surface has been studied by Shreedevi et al. [8], who have mixed both carbon nanotubes and silver nanoparticles in the base fluid (water). The effect of thermal radiation and suction concerning the dynamics of an MHD hybrid nanofluid as it moves through a stretching/shrinking sheet, with particular emphasis on the heat transfer, has been investigated very recently by Yashkun et al. [9]. It has been shown by his findings that the hybrid nanofluid ($Cu - Al_2O_3$/water) is more efficient than the nanofluid (Cu/water) for the heat transfer phenomena. An analytical approach to study the heat transfer phenomena of an unsteady hybrid nanofluid flow past an infinite flat vertical plate has been made by Rajesh et al. [10]. The effect of heat transfer and magnetic field in the flow of Casson hybrid nanofluid, composed by mixing the nanoparticles of copper oxide and graphite oxide in methanol over a vertical stretching sheet, has been investigated by Alkasasbeh [11]. The interaction between the flow of hybrid nanofluid and melting heat transfer considering the effect of second-order slip, Eckert number, and Prandtl number has been studied by Jawad et al. [12] over a stretching surface. Yaseen et al. [13] made

an investigation on how MHD radiative hybrid nanofluids, such as MoS_2-SiO_2/kerosene oil and MoS_2/kerosene oil, behave between shrinking and rotating disks. It examines heat transfer using the Cattaneo–Christov heat flux model, convective heating, and magnetic fields. Recent work on hybrid nanofluid is included in the literature cited in Ref. [14–17].

The effect of thermal radiation on natural convection has risen in prominence due to its many practical applications in engineering and physics, especially in the development of tools and machinery, aerospace engineering, and gas turbines. Since it does not need a medium, thermal radiation is the preferred mode of heat transmission above conduction and convection. Because of these characteristics, thermal radiation plays a crucial role in the heat transmission of MHD nanofluids, minimising heat loss. In the early stage, the impact of heat radiation on Air and CO_2 of laminar flow through the vertical plate was studied by England and Emery [18]. The effects of radiation and viscous dissipation on the thermal boundary layer over a nonlinearly stretching sheet were investigated by Cortell [19]. The impact of thermal radiation on the motion of an MHD nanofluid in an unsteady state caused by a stretching sheet was analysed by Shakhaoath et al. [20]. A model was developed by Kumar et al. [21] to simulate the flow and heat transfer of a nanofluid across an infinite vertical plate subject to a magnetic field and viscous dissipation. Details of impact made by thermal radiation on MHD hybrid nanofluid flow along the stretching cylinder was studied in subsequent research by Ali et al. [22]. In a situation where the bottom plate was permeable and stretchy, the impact of thermal radiation, hall current, and uneven heat source/sink on the flow of nanofluid between two horizontal flat plates was investigated by Lv et al. [23]. The effect of thermal radiation and chemical reactions on MHD Casson nanofluid flow caused by a stretching sheet was considered by Rao and Deka [24]. The flow behaviour of unsteady Casson nanofluid over a stretching sheet with the effect of solar thermal radiation was studied by Jamshed et al. [25]. A numerical investigation on the heat and mass transfer phenomena of a nanofluid under the impact of solar radiation has been conducted by Rao and Deka [26]. Some recent contributions to the flow of hybrid nanofluid under the effect of thermal radiation are included in ref. [27–32].

The objective of this study is to investigate the influence of magnetic field, thermal radiation Joule heating and viscous dissipation with different slip flow effects such as velocity and thermal slips in the flow of hybrid nanofluid past a non-linear stretching sheet with porous medium. Initially, the Ag nanoparticles of volume fraction ($\phi_1 = 0.01$) are suspended on the base fluid to form the Ag/water nanofluid. Again, Al_2O_3 nanoparticles of volume fraction ($\phi_2 = 0.02$) are added to the Ag/water nanofluid to form the $Ag - Al_2O_3$/water hybrid nanofluid. The motivation for utilizing a hybrid nanofluid, consisting of silver (Ag) and alumina (Al_2O_3) nanoparticles in water (H_2O), is based on the expectation of synergistic effects. This combination allows for tailored nanofluid properties, particularly enhancing thermal boundary layer control in two-dimensional time-independent MHD flow and heat transfer. The superior performance of the hybrid nanofluid over single-component nanofluids is aimed to be showcased by the study, emphasizing improved heat transfer characteristics and fluid speed control through external factors like magnetic fields and porous media. The governing partial differential equations are transformed into ordinary differential equations and then solved numerically by an implicit finite difference method known as the Keller-box method. To prove the validity of the numerical approach the numerical results have been compared with the previous results of Wang et al. [33], Gorla and Sidawi [34], Khan and Pop [4], Devi and Devi [35] and Waini et al. [7] for certain cases and it is observed that all the results are in excellent agreement. The study also shows the behaviour of $Ag - water$ nanofluid to draw a better comparison of hybrid nanofluid ($Ag - Al_2O_3/water$) with that of nanofluid ($Ag - water$).

Mathematical Formulation

Let us consider a steady flow and heat transfer of a $Ag-Al_2O_3/water$ based hybrid nanofluid with a slip effect through a permeable stretched surface as shown in Fig. 1. The x-axis is measured along the sheet whereas the y-axis is taken normal to the sheet. The sheet is stretched with the rate of 'c' resulting the fluid to flow with a speed of $u_o = cx$. When time $t > 0$ passed, the temperature increased to their maximum values of $T_w(> T_\infty)$ and remained stable thereafter, here T_w denote the temperature near the wall, and T_∞ those away from the confines of the wall. In the direction of y-axis, a magnetic field B_0 is applied. Considering that the fluid is slightly conducting, the magnetic Reynolds number is much less than unity, and thus the induced magnetic field is negligible when compared to the applied magnetic field. In addition, velocity slip and thermal slip are taken into consideration at the wall. The thermophysical properties of water and nanoparticles are discussed in Table 1. Table 2 provides the thermophysical properties model for hybrid nanofluid.

The following equations describe the MHD hybrid nanofluid flow with heat transfer under the aforementioned assumptions and the standard boundary conditions [9] [17]:

$$\frac{\partial u}{\partial x} + \frac{\partial v}{\partial y} = 0, \tag{1}$$

$$u\frac{\partial u}{\partial x} + v\frac{\partial u}{\partial y} = \frac{\mu_{hnf}}{\rho_{hnf}}\frac{\partial^2 u}{\partial y^2} - \frac{\sigma_{hnf}}{\rho_{hnf}}B_o^2 u - \frac{\mu_{hnf}}{\rho_{hnf}}\frac{u}{k_o}, \tag{2}$$

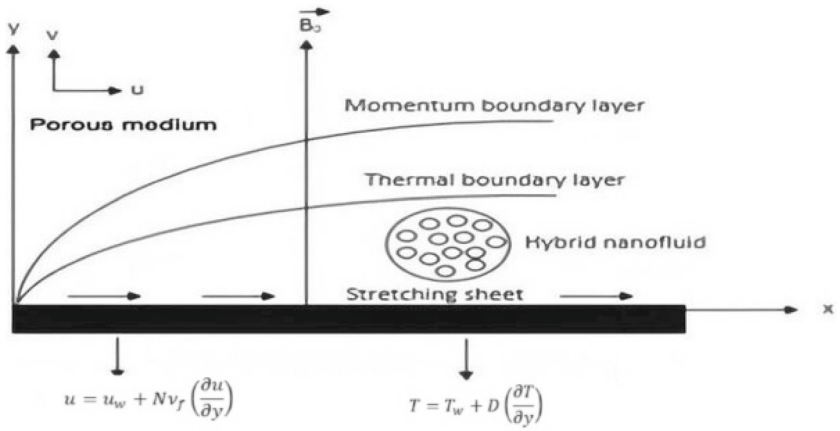

Fig. 1 Schematic diagram of the problem

Table 1 Thermophysical properties of water and nanoparticles

	$\rho(kg/m^3)$	$\kappa(W/mK)$	$\sigma(s/m)$	$C_p(J/kgK)$
H_20	997.1	0.613	5.5×10^{-6}	4179
Ag	10500	429	6.30×10^7	235
Al_2O_3	3970	40	35×10^6	765

Table 2 Thermophysical properties model for hybrid nanofluid [35]

Property	Hybrid nanofluid
Density	$\rho_{hnf} = (1-\phi_2)\left[(1-\phi_1)\rho_f + \phi_1\rho_{s1}\right] + \phi_2\rho_{s2}$
Dynamic viscosity	$\mu_{hnf} = \frac{\mu_f}{(1-\phi_1)^{2.5}(1-\phi_2)^{2.5}}$
Heat Capacity	$(\rho C_p)_{hnf} = (1-\phi_2)\left[(1-\phi_1)(\rho C_p)_f + \phi_1(\rho C_p)_{s1}\right] + \phi_2(\rho C_p)_{s2}$
Thermal Conductivity	$\kappa_{hnf} = \frac{\kappa_{s2}+2\kappa_{nf}-2\phi_2(\kappa_{nf}-\kappa_{s2})}{\kappa_{s2}+2\kappa_{nf}+\phi_2(\kappa_{nf}-\kappa_{s2})} \times \kappa_{nf}$
	$where,\ \kappa_{nf} = \frac{\kappa_{s1}+2\kappa_f-2\phi_1(\kappa_f-\kappa_{s1})}{\kappa_{s1}+2\kappa_f+\phi_1(\kappa_f-\kappa_{s1})} \times \kappa_f$
Electrical conductivity	$\sigma_{hnf} = \frac{\sigma_{s2}(1+2\phi_2)+2\sigma_{hf}(1-\phi_2)}{\sigma_{s2}(1-\phi_2)+\sigma_{nf}(2+\phi_2)} \times \sigma_{nf}$
	$where,\ \sigma_{nf} = \frac{\sigma_{s1}(1+2\phi_1)+2\sigma_f(1-\phi_1)}{\sigma_{s1}(1-\phi_1)+\sigma_f(2+\phi_1)} \times \sigma_f$

$$u\frac{\partial T}{\partial x} + v\frac{\partial T}{\partial y} = \frac{\kappa_{hnf}}{(\rho C_p)_{hnf}}\frac{\partial^2 T}{\partial y^2} + \frac{\mu_{hnf}}{(\rho C_p)_{hnf}}\left(\frac{\partial u}{\partial y}\right)^2 + \frac{\sigma_{hnf}}{(\rho C_p)_{hnf}}B_o^2 u^2 - \frac{1}{(\rho C_p)_{hnf}}\frac{\partial q_r}{\partial y}, \tag{3}$$

The following are the initial and boundary conditions [36, 37]:

$$u = u_w + N\mu_{hnf}\left(\frac{\partial u}{\partial y}\right),\ v = 0,\ T = T_w + D\kappa_{hnf}\left(\frac{\partial T}{\partial y}\right) asy = 0,$$
$$u \to 0,\ v \to 0,\ T \to T_\infty asy \to \infty, \tag{4}$$

where, $u_w = cx$, N is the velocity slip factor and D is the thermal slip factor. Here, both N and D are constant function and a no-slip condition can be obtained when $N = D = 0$.

The Rosseland approximation for radiative heat flux can be mathematically written as [38–40] –

$$q_r = \frac{-4\sigma^*}{3k^*}\frac{\partial T^4}{\partial y}, \tag{5}$$

By generalizing the Taylor series and ignoring the higher order terms, we are able to get

$$T^4 = 4\,T_\infty^3\,T - 3\,T_\infty^4,$$

Hence Eq. (5) becomes-

$$\frac{\partial q_r}{\partial y} = \frac{-16\sigma^*}{3k^*}\,T_\infty^3\,\frac{\partial^2 T}{\partial y^2}, \tag{6}$$

We use the similarity transformation [7]-

$$\eta = \sqrt{\frac{c}{\nu_f}}y,\ u = cxf'(\eta),\ v = -\sqrt{c\nu_f}f(\eta),\ \theta = \frac{T-T_\infty}{T_w-T_\infty}, \tag{7}$$

Substituting Eq. (7) in the governing Eqs. (1) to (3) we get:

$$f''' + \frac{A_2}{A_1}ff'' - \frac{A_2}{A_1}f'^2 - \left(\frac{MA_5}{A_1} + K_p\right)f' = 0, \tag{8}$$

$$\frac{\theta''}{Pr}\left(A_4+\frac{4}{3}R\right)+A_3 f\theta\prime+A_1 Ecf''^2+A_5 MEcf'^2=0, \tag{9}$$

The boundary condition given in Eq. (4) is transformed to:

$$f(0)=0,\ f\prime(0)=1+\lambda f''(0),\ \theta(0)=1+\delta\theta\prime(0),\ f'(\infty)\to 0,\ \theta(\infty)\to 0, \tag{10}$$

In this study, we specify the flow parameters as follows -

$$A_1=\frac{\mu_{hnf}}{\mu_f},\ A_2=\frac{\rho_{hnf}}{\rho_f},\ A_3=\frac{(\rho C_p)_{hnf}}{(\rho C_p)_f},\ A_4=\frac{\kappa_{hnf}}{\kappa_f},\ A_5=\frac{\sigma_{hnf}}{\sigma_f},$$
$$M=\frac{\sigma_f B_o^2}{c\rho_f},\ K_p=\frac{\nu_f}{ck_o},\ Pr=\frac{\nu_f(\rho C_p)_f}{\kappa_f},\ R=\frac{4T_\infty^3\sigma^*}{\kappa_f k^*},\ Ec=\frac{c^2x^2}{C_p(T_w-T_\infty)},$$
$$\lambda=N\mu_{hnf}\sqrt{\frac{c}{\nu_f}},\ \delta=D\kappa_{hnf}\sqrt{\frac{c}{\nu_f}},$$

Combining velocity slip parameter (λ) and thermal slip parameter (δ) we get-

$$\text{CombinedSlip}=c\times\frac{\mu_{hnf}}{\rho_{hnf}}\times\frac{\kappa_{hnf}}{(\rho C_p)_{hnf}}$$

The following physical quantities are observed in this study that are very important in area of engineering sciences and industrial processes. The skin friction coefficient (C_f) and the Nusselt number (Nu_x) are defined as follows-

$$Cf_x=\frac{\tau_w}{\rho_f u_w^2}, \tag{11}$$
$$Nu_x=\frac{xq_w}{\kappa_f(T_w-T_\infty)}, \tag{12}$$

where

$$\tau_w=\mu_{hnf}\left(\frac{\partial u}{\partial y}\right)_{y=0} and q_w=-\kappa_{hnf}\left(\frac{\partial T}{\partial y}\right)_{y=0}+(q_r)_{y=0} \tag{13}$$

Substituting Eq. (13) into Eqns. (11) to (12) we get-

$$\text{Re}_x^{\frac{1}{2}}Cf_x=\frac{1}{(1-\phi_1)^{2.5}(1-\phi_2)^{2.5}}f''(0),$$
$$\text{Re}_x^{-\frac{1}{2}}Nu_x=-\left[\frac{\kappa_{hnf}}{\kappa_f}+\frac{4}{3}R\right]\theta\prime(0)$$

where $\text{Re}_x=\frac{xu_w}{\nu_f}$ stands for local Reynolds number.

"The Keller-box technique is used to numerically solve Eqs. (8) and (9), together with Boundary Condition in Eq. (10). We chose this scheme because of its flexibility and it is found to be very effective in solving the non-linear problem with an error of order 10^{-5}. Methodology from Cebeci and Bradshaw [41] has been implemented. Computational steps (which were clearly explained by Anwar et al. [42]) involved in this scheme to get a numerical solution are as follows:

a) To reduce the obtained ordinary differential equations (ODE) into the system of first-order equations.
b) To write the reduced equations in finite difference.
c) To linearize the equations using Newton's method and write them in vector form.

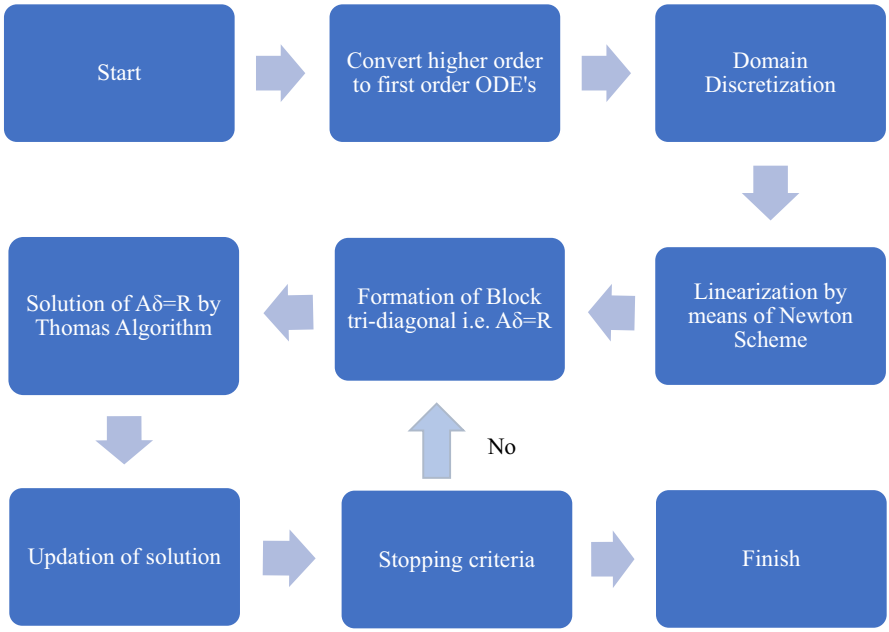

Fig. 2 Flow chart illustrating the Keller-box method

d) To solve the linear equations which involve the tri-diagonal matrix. The flow chart of the Keller-box method is displayed in Fig. 2.

Results and Discussion

To study the physical representation of the problem, the numerical results are reported in both graphical as well as in tabular form. The influence of various parameters on the velocity profile and temperature profile are plotted in graphs whereas the numerical values of the skin-friction coefficient and Nusselt number are presented in tables. Here all the graphs and the numerical values are obtained by implementing the Keller-box method using MATLAB code. In an attempt to check the validity of the results obtained a comparison is made with those of previously reported results of Wang et al. [33], Gorla and Sidawi [34], Khan and Pop [4], Devi and Devi [35], and Waini et al. [7]. Table 3 seems to be in excellent compliance and higher accuracy. Therefore, we are confident that our results are reliably accurate to address the problem.

Table 4 intends to draw a comparison of our results with that of Devi and Devi [35] and Waini et al. [7] for the values of $Cf_x Re_x^{\frac{1}{2}}$ and $Nu_x Re_x^{-\frac{1}{2}}$ for $Cu - Al_2O_3/water$ hybrid nanofluid for different values of ϕ_2."

The changes in velocity of both hybrid nanofluid $(Ag - Al_2O_3/water)$ and nanofluid $(Ag/water)$ for various values of M are shown in Fig. 3. It is seen here that for both cases, the velocity decreases as the magnetic parameter rises. It can also be observed that $Ag/water$ nanofluid flow is slightly slower than the $Ag - Al_2O_3/water$ hybrid nanofluid flow. When the magnetic field becomes stronger, a retarding force called the Lorentz force is produced,

Table 3 Comparison for values of $-\theta\prime(0)$ for ordinary fluid ($\phi_1 = 0 and \phi_2 = 0$) with various values of Pr when $\lambda = \delta = M = R = Ec = Kp = 0$

Pr	Wang et al. [33]	Gorla and Sidawi [34]	Khan and Pop [4]	Devi and Devi [35]	Waini et al. [7]	Present
2	0.9114	0.9114	0.9113	0.91135	0.911353	0.9114
6.13	–	–	–	1.75968	1.759682	1.7597
7	1.8954	1.8954	1.8954	1.89540	1.895400	1.8954
20	3.3539	3.3539	3.3539	3.35390	3.353902	3.3540

Table 4 Values of $Cf_x Re_x^{\frac{1}{2}}$ and $Nu_x Re_x^{-\frac{1}{2}}$ for $Cu - Al_2O_3/water$ hybrid nanofluid for different values of ϕ_2 when $\phi_1 = 0.1$, $\lambda = 1$, and $Pr = 6.135$

ϕ_2	$Cf_x Re_x^{\frac{1}{2}}$			$Nu_x Re_x^{-\frac{1}{2}}$		
	Devi and Devi [35]	Waini [7]	Present	Devi and Devi [35]	Waini [7]	Present
0.005	− 1.327310	− 1.327098	− 1.3271	1.961686	1.961773	1.9618
0.02	− 1.409683	− 1.409490	− 1.4094	1.989226	1.989308	1.9893
0.04	− 1.520894	− 1.520721	− 1.5206	2.026368	2.026446	2.0265
0.06	− 1.634279	− 1.634119	− 1.6341	2.064075	2.064150	2.0640

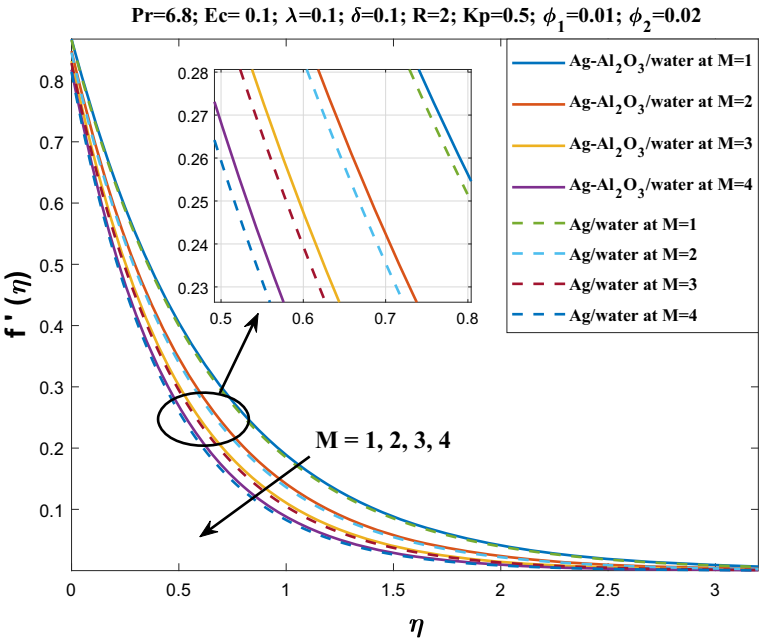

Fig. 3 Velocity profile for different value of M

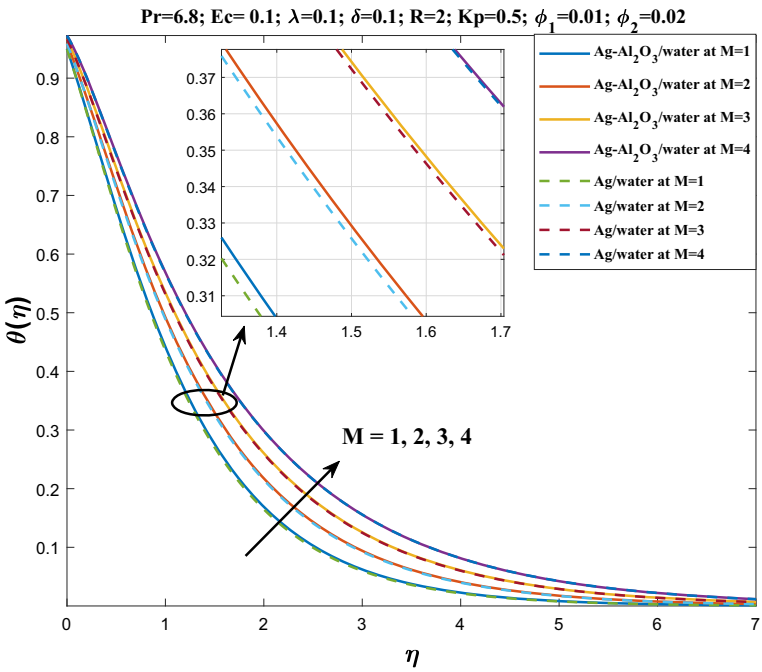

Fig. 4 Temperature profile for different value of M

which causes the flow to slow down. This is why the velocity profile decreases as M rises. It can be shown in Fig. 4 that as M is raised, so too is the range of temperatures experienced inside the boundary layer. The temperature in the boundary layer area rises as a result of increased frictional resistance to the flow brought on by an increase in the Lorentz force. Therefore, a temperature increase results from an increase in M. It was clear from the figure that the $Ag - Al_2O_3/water$ hybrid nanofluid holds temperature better than the $Ag/water$ nanofluid.

Figure 5 and 6 reveal the impact of K_p on the velocity and temperature profile respectively. It is clear from the figures that the velocity for both $Ag - Al_2O_3/water$ hybrid nanofluid and $Ag/water$ nanofluid decrease with the increase in the value of K_p whereas an opposite behaviour is observed for the temperature profile of both cases. When the value of K_p increases, the porous layer expands, which reduces the Darcian body force and hence results in slower fluid flow. Moreover, the porosity parameter in a nanofluid includes internal heat generation, which causes the temperature to rise in the fluid. The porosity parameter is defined as the ratio of the void volume to the total volume of the nanofluid. As a result, when the porosity parameter increases, the internal heat generation within the nanofluid also increases, which causes an increase in temperature. From the figure, it can be concluded that the hybrid nanofluid shows better results in controlling the velocity as well as holding the temperature for this instance.

Figure 7 exhibit the effect of Pr on dimensionless temperature for both $Ag-Al_2O_3/water$ hybrid nanofluid and $Ag/water$ nanofluid. As Pr rises, it's easy to see how the temperature within the boundary layer area drops. The Prandtl number (Pr) is the ratio of momentum diffusivity to thermal diffusivity. When the Prandtl number increases, the heat transfer rate

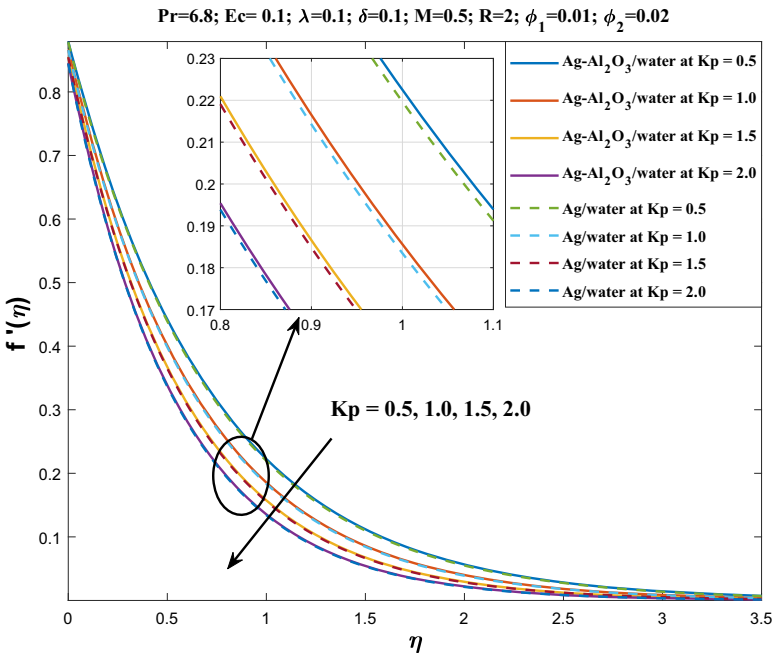

Fig. 5 Velocity profile for different value of K_p

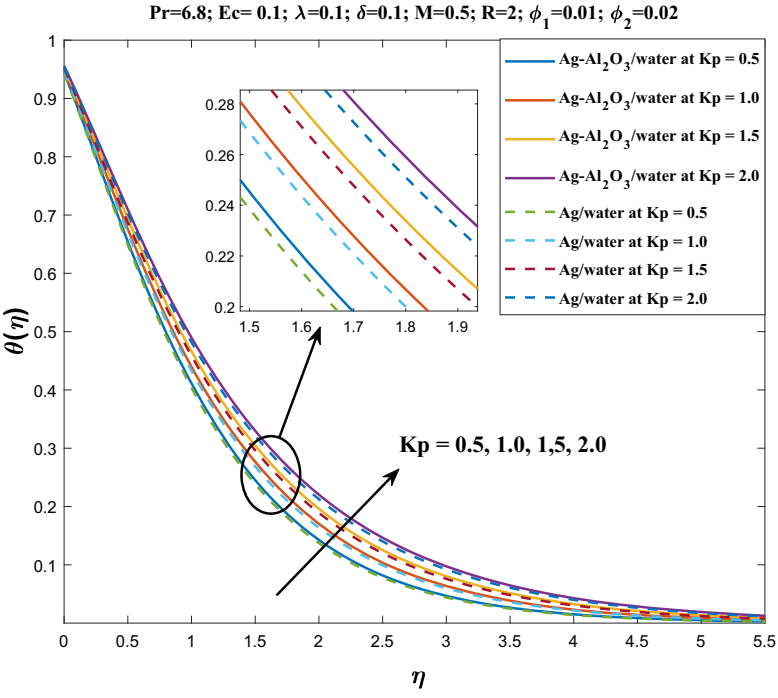

Fig. 6 Temperature profile for different value of K_p

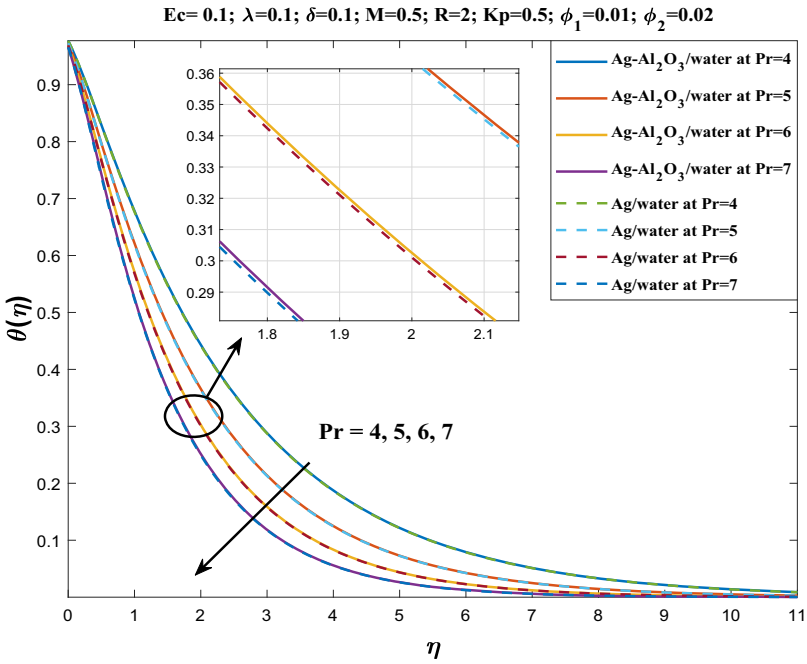

Fig. 7 Temperature profile for different value of Pr

of the fluid increases, which causes the temperature of the boundary layer to decrease. This is because the thermal diffusivity of the fluid is lower than the momentum diffusivity, which means that heat is transferred more slowly than momentum. The impact of radiation parameter (Rd) on the temperature profile is shown in Fig. 8. The figure shows the impact for both $Ag-Al_2O_3/water$ hybrid nanofluid and $Ag/water$ nanofluid and it is evident that when the radiation parameter increases, the temperature rises. The reason for the observed phenomenon is due to the release of heat energy into the fluid resulting from an increase in thermal radiation.. It is noteworthy to see that the hybrid nanofluid shows a higher temperature profile than the ordinary nanofluid.

The relationship between Eckert number and temperature profile is seen in Fig. 9. The dimensionless temperature rises as Ec rises, as can be seen in both $Ag-Al_2O_3/water$ hybrid nanofluid as well as $Ag/water$ nanofluid. Ec is a dimensionless quantity that represents the ratio of kinetic energy to the thermal energy of a fluid. When the Ec increases, the kinetic energy of the fluid increases relative to its thermal energy. This means that the fluid is able to convert more of its kinetic energy into heat energy, which causes the temperature to rise.

The influence of the velocity slip parameter (λ) on the velocity profile is seen in Fig. 10. Observations indicate that the dimensionless velocity profile decreases as λ increases. λ is a dimensionless quantity that represents the ratio of the molecular mean free path to a characteristic length scale of the flow. When the λ increases, the mean free path becomes more significant relative to the characteristic length scale of the flow. This leads to an increase in the velocity slip at the fluid–solid interface. As a result of the increased velocity slip, the fluid velocity near the solid surface decreases. This is because the velocity slip reduces the amount of momentum transfer between the fluid and the solid surface, which causes the fluid

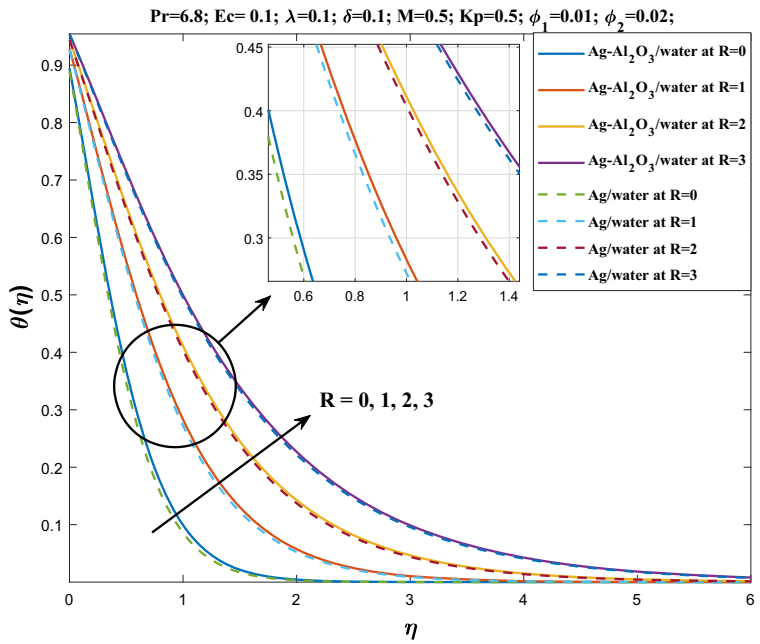

Fig. 8 Temperature profile for different value of R

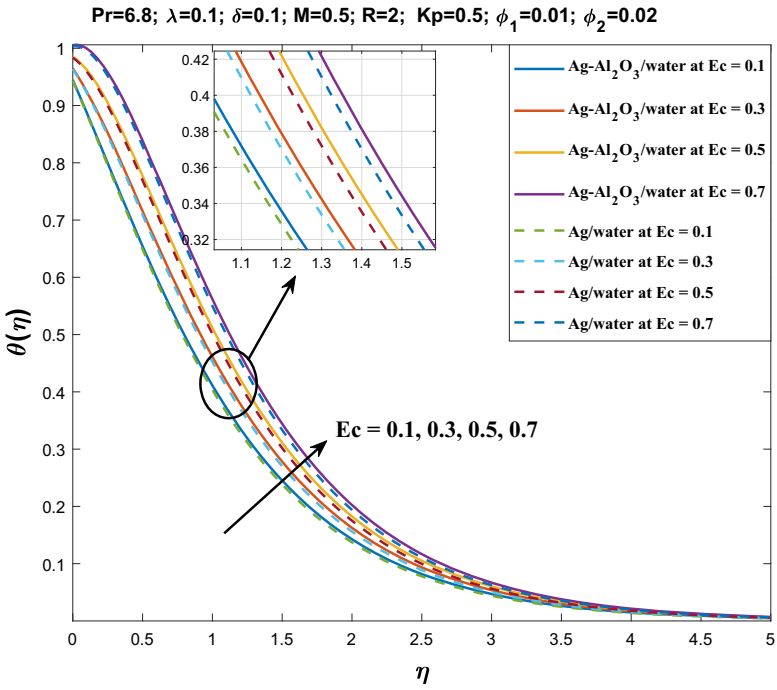

Fig. 9 Temperature profile for different value of Ec

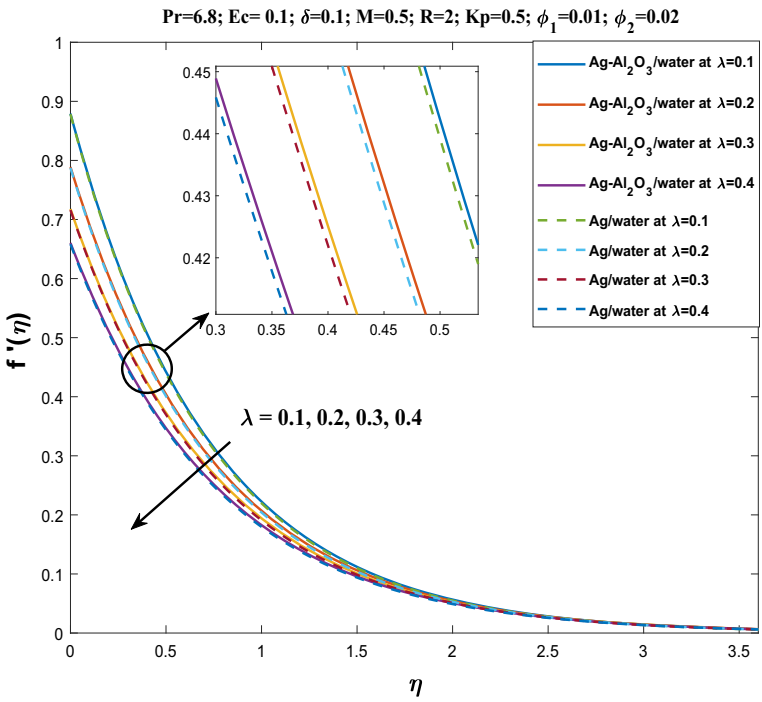

Fig. 10 Velocity profile for different value of λ

velocity to decrease near the surface. Therefore, an increase in the velocity slip parameter leads to a decrease in the velocity profile near the solid surface.

In Fig. 11 we see how the thermal slip parameter (δ) affects the temperature distribution. Raising the values of δ decreases the temperature. δ is a dimensionless quantity that represents the ratio of the molecular mean free path for heat transfer to a characteristic length scale of the flow. When the thermal slip parameter increases, the mean free path becomes more significant relative to the characteristic length scale of the flow. This leads to an increase in the thermal slip at the fluid–solid interface. As a result of the increased thermal slip, the temperature gradient near the solid surface decreases. This is because the thermal slip reduces the amount of heat transfer between the fluid and the solid surface, which causes the temperature gradient to decrease near the surface. Therefore, an increase in the thermal slip parameter leads to a decrease in the temperature profile near the solid surface.

Figures 12 and 13 reflect the influence of temperature profile for the increasing value of ϕ_1 and ϕ_2 respectively. It is clear from the figures that the temperature intensifies with the increases in the volume fraction of both nanoparticle of the hybrid nanofluid. When the volume fraction of nanoparticles is increased, there is a greater chance for the nanoparticles to come into contact with each other and form clusters or agglomerates. These clusters can then act as heat sources, which can increase the temperature of the nanofluid.

The Effect of K_p on $-f''(0)$ for different values of M is presented in Fig. 14. It can be observed that the trends of $-f''(0)$ keep increasing with the increase in both M and K_P for both $Ag - Al_2O_3/water$ hybrid nanofluid as well as $Ag/water$ nanofluid. Lastly, Fig. 15 depicts the influence of M on $-\theta'(0)$ for different values of Rd. It is noteworthy to see from

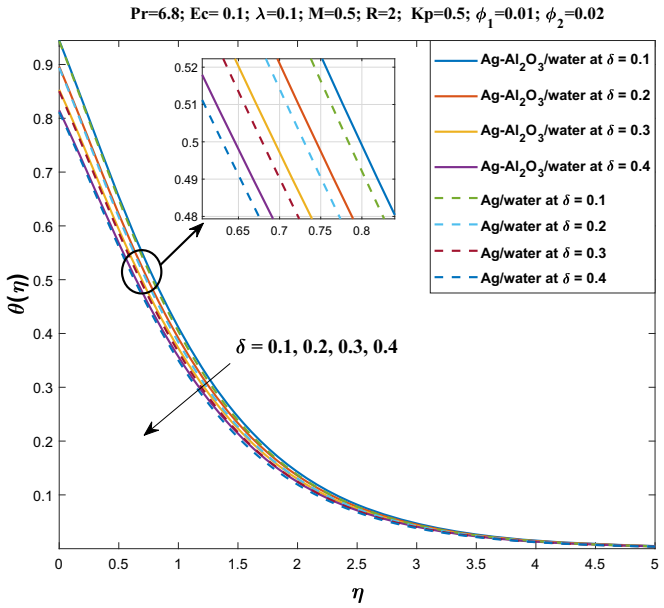

Fig. 11 Temperature profile for different value of δ

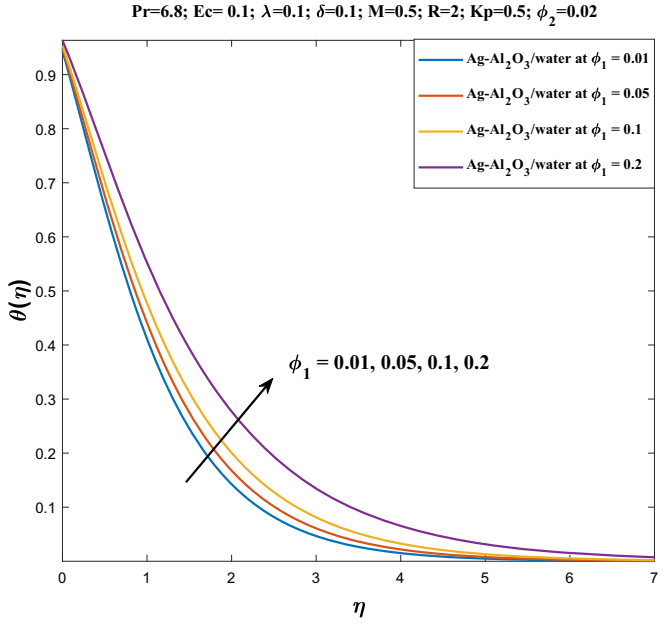

Fig. 12 Temperature profile for different value of ϕ_1

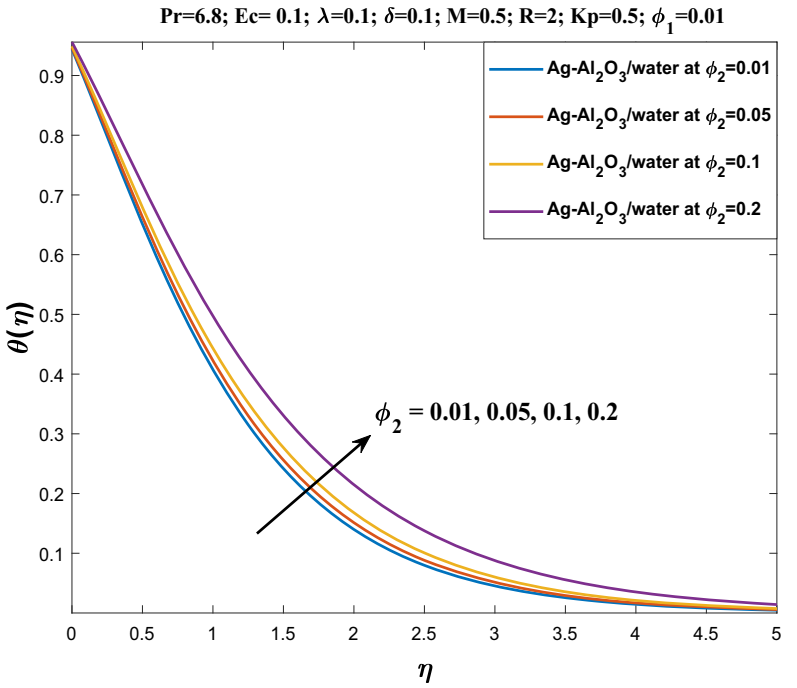

Fig. 13 Temperature profile for different value of ϕ_2

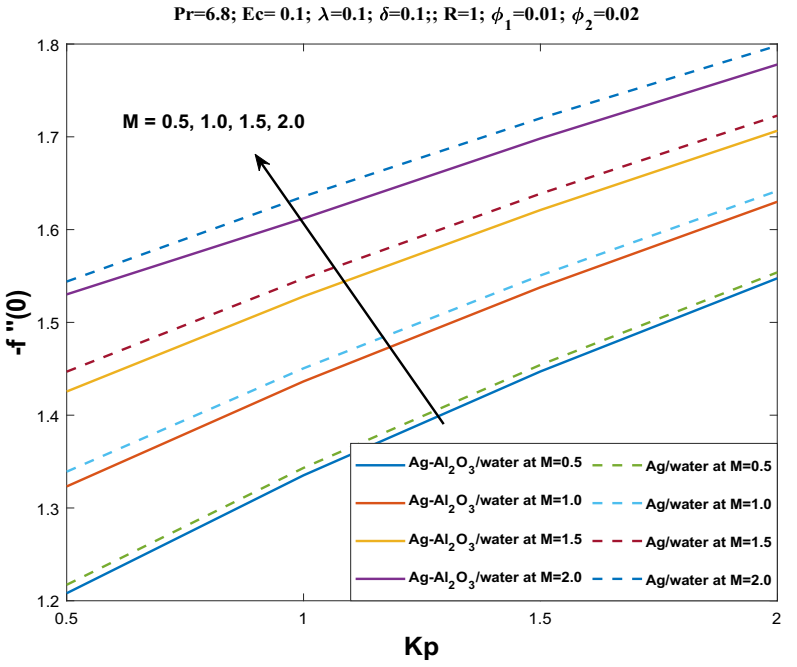

Fig. 14 Effect of Kp on $-f''(0)$ profile for different value of M

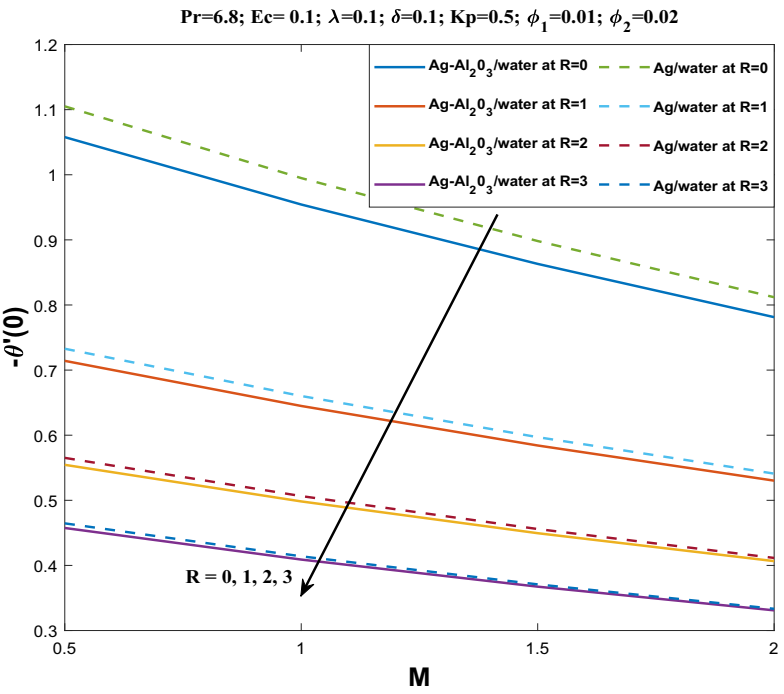

Fig. 15 Effect of M on $\theta\prime(0)$ profile for different value of R

the plottings that $-\theta\prime(0)$ continuously lowers as the value of both Rd and M rises for both the case of $Ag - Al_2O_3/water$ hybrid nanofluid and $Ag/water$ nanofluid.

Conclusion

Considering the slip effect, heat transfer of a two-dimensional MHD hybrid nanofluid flow over a porous stretching sheet is numerically analysed in this article. The equations are solved using the Keller-box method. This method is highly accurate for parabolic problems. We have used this scheme because it is quite flexible among most of the other schemes. The accuracy of the numerical approach is validated against some previously published work and the results show an excellent agreement. The finding from the study is drawn as follows:

1. The velocity of the hybrid nanofluid flow inside the boundary layer region can be controlled by increasing the effect of magnetic field, porosity and boundary slip.
2. The temperature of the boundary layer region is enhanced with the increase in the effect of the magnetic field, porosity, thermal radiation, viscosity and volume fraction of the nanoparticles used.
3. The temperature of the hybrid nanofluid starts depleting with the increase in the value of the Prandtl number and thermal slip parameter.
4. The flow of nanofluid with single nanoparticles is found to be slightly slower than that of the hybrid nanofluid.

5. The boundary layer region of the hybrid nanofluid is found to be warmer than the nanofluid with single nanoparticles.
6. The use of hybrid nanofluid gives better results than that of the nanofluid with single nanoparticles.

Author contributions Rao wrote the main manuscript text with all tables. Deka prepared all the figures. All the aurthour reviewed the manuscript.

Funding This research received no specific grant from any funding agency in the public, commercial, or notfor- profit sectors.

Data availability Not applicable.

Declarations

Conflict of interest The authors declare no competing interests.

References

1. Choi, S.U.S.: Enhancing thermal conductivity of fluids with nanoparticles. ASME Int. Mech. Eng. Congr. Expos. **66**, 99–105 (1995)
2. Buongiorno, J.: Convective transport in nanofluids. J. Heat Transf. **128**(3), 240–250 (2006)
3. Nield, D.A., Kuznetsov, A.V.: Thermal instability in a porous medium layer saturated by a nanofluid. Int. J. Heat Mass Transf. **52**(25–26), 5796–5801 (2009)
4. Khan, W.A., Pop, I.: Boundary-layer flow of a nanofluid past a stretching sheet. Int. J. Heat Mass Transf. **53**(11), 2477–2483 (2010)
5. Makinde, O.D., Aziz, A.: Boundary layer flow of a nanofluid past a stretching sheet with a convective boundary condition. Int. J. Therm. Sci. **50**(7), 1326–1332 (2011)
6. Sundar, L.S., Sharma, K.V., Singh, M.K., Sousa, A.C.M.: Hybrid nanofluids preparation, thermal properties, heat transfer and friction factor-A review. Renew. Sustain. Energy Rev. **68**, 185–198 (2017)
7. Waini, I., Ishak, A., Pop, I.: Unsteady flow and heat transfer past a stretching/shrinking sheet in a hybrid nanofluid. Int. J. Heat Mass Transf. **136**, 288–297 (2019)
8. Sreedevi, P., Sudarsana Reddy, P., Chamkha, A.: Heat and mass transfer analysis of unsteady hybrid nanofluid flow over a stretching sheet with thermal radiation. SN Appl. Sci. **2**, 1222 (2020)
9. Yashkun, U., Zaimi, K., Abu Bakar, N.A., Ishak, A., Pop, I.: MHD hybrid nanofluid flow over a permeable stretching/shrinking sheet with thermal radiation effect. Int. J. Numer. Meth. Heat Fluid Flow **31**(3), 1014–1031 (2021)
10. Rajesh, V., Sheremet, M.A., Öztop, H.F.: Impact of hybrid nanofluids on MHD flow and heat transfer near a vertical plate with ramped wall temperature. Case Stud. Thermal Eng. **28**, 101557 (2021)
11. Alkasasbeh, H.: Numerical solution of heat transfer flow of casson hybrid nanofluid over vertical stretching sheet with magnetic field effect. CFD Lett. **14**(3), 39–52 (2022)
12. Jawad, Md., Khan, Z., Bonyah, E., Jan, R.: Analysis of hybrid nanofluid stagnation point flow over a stretching surface with melting heat transfer. Math. Probl. Eng. **2022**, 9469164 (2022)
13. Yaseen, M., Rawat, S.K., Kumar, M.: Cattaneo-Christov heat flux model in Darcy-Forchheimer radiative flow of MoS2–SiO2/kerosene oil between two parallel rotating disks. J. Therm. Anal. Calorim. **147**, 10865–10887 (2022)
14. Rao, S., & Deka, P. N. (2023). A study on MHD flow of SWCNT-Al2O3/water hybrid nanofluid past a vertical permeable cone under the influence of thermal radiation and chemical reactions. Numer. Heat Transf. Part A Appl. 1–21
15. Sajid, T., Gari, A.A., Jamshed, W., Eid, M.R., Islam, N., Irshad, K., Altamirano, G.C., El Din, S.M.: Case study of autocatalysis reactions on tetra hybrid binary nanofluid flow via Riga wedge: biofuel thermal application. Case Stud. Thermal Eng. **47**, 103058 (2023)
16. Kai, Y., Ali, K., Ahmad, S., Ahmad, S., Jamshed, W., Raizah, Z., El Din, S.M.: A case study of different magnetic strength fields and thermal energy effects in vortex generation of Ag-TiO_2 hybrid nanofluid flow. Case Stud. Thermal Eng. **47**, 103115 (2023)

17. Rao, S., Deka, P.: Analysis of MHD bioconvection flow of a hybrid nanofluid containing motile microorganisms over a porous stretching sheet. BioNanoScience **13**, 2134–2150 (2023)
18. Cortell, R.: Effects of viscous dissipation and radiation on the thermal boundary layer over a nonlinearly stretching sheet. Phys. Lett. A **372**(5), 631–636 (2008)
19. England, W.G., Emery, A.F.: Thermal radiation effects on the laminar free convection boundary layer of an absorbing gas. ASME. J. Heat Transf. **91**(1), 37–44 (1969)
20. Khan, M.S., Alam, M.M., Tzirtzilakis, E.E., Ferdows, M., Karim, I.: Finite difference simulation of MHD radiative flow of a nanofluid past a stretching sheet with stability analysis. Int. J. Adv. Thermofluid Res. **2**, 31–46 (2016)
21. Kumar, M.A., Reddy, Y.D., Rao, V.S., Goud, B.S.: Thermal radiation impact on MHD heat transfer natural convective nano fluid flow over an impulsively started vertical plate. Case Stud. Thermal Eng. **24**, 100826 (2021)
22. Ali, A., Kanwal, T., Awais, M., Shah, Z., Kumam, P., Thounthong, P.: Impact of thermal radiation and non-uniform heat flux on MHD hybrid nanofluid along a stretching cylinder. Sci. Rep. **11**(1), 1–14 (2021)
23. Lv, Y., Shaheen, N., Ramzan, M., Mursaleen, M., Nisar, K.S., Malik, M.Y.: Chemical reaction and thermal radiation impact on a nanofluid flow in a rotating channel with Hall current. Sci. Rep. **11**(1), 1–17 (2021)
24. Rao, S., Deka, P.: A numerical solution using EFDM for unsteady MHD radiative Casson nanofluid flow over a porous stretching sheet with stability analysis. Heat Transfer **51**(8), 8020–8042 (2022)
25. Jamshed, W., Uma Devi, S.S., Goodarzi, M., Prakash, M., Sooppy Nisar, K., Zakarya, M., Abdel-Aty, A.: Evaluating the unsteady Casson nanofluid over a stretching sheet with solar thermal radiation: an optimal case study. Case Stud. Thermal Eng. **26**, 101160 (2021)
26. Rao, S., Deka, P.N.: A Numerical Investigation on Transport Phenomena in a Nanofluid Under the Transverse Magnetic Field Over a Stretching Plate Associated with Solar Radiation. In: Banerjee, S., Saha, A. (eds.) Nonlinear Dynamics and Applications, pp. 473–492. Springer Proceedings in Complexity, Springer, Cham (2022)
27. Jamshed, W., Aziz, A.: A comparative entropy based analysis of Cu and Fe_3O_4/methanol Powell-Eyring nanofluid in solar thermal collectors subjected to thermal radiation, variable thermal conductivity and impact of different nanoparticles shape. Results Phys. **9**, 195–205 (2018)
28. Jamshed, W., Nisar, K.S., Ibrahim, R.W., Mukhtar, T., Vijayakumar, V., Ahmad, F.: Computational frame work of Cattaneo-Christov heat flux effects on Engine Oil based Williamson hybrid nanofluids: a thermal case study. Case Stud. Thermal Eng. **26**, 101179 (2021)
29. Das, B.R., Deka, P., Rao, S.: Numerical analysis on MHD mixed convection flow of Al_2O_3/H_2O (Aluminum-Water) nanofluids in a vertical square duct. East Eur. J. Phys. **2**, 51–62 (2023)
30. Rao, S., Deka, P.: A numerical study on heat transfer for MHD flow of radiative casson nanofluid over a porous stretching sheet. Latin Am. Appl. Res. Int. J. **53**(2), 129–136 (2023)
31. Zhang, X., Yang, D., Katbar, N.M., Jamshed, W., Ullah, I., Eid, M.R., Raizah, Z., Ibrahim, R.W., El-Wahed Khalifa, H.A., El Din, S.M.: Entropy and thermal case description of monophase magneto nanofluid with thermal jump and Ohmic heating employing finite element methodology. Case Stud. Thermal Eng. **45**, 102919 (2023)
32. Rao, S., Deka, P.N.: A numerical study on unsteady mhd williamson nanofluid flow past a permeable moving cylinder in the presence of thermal radiation and chemical reaction. Biointerface Res. Appl. Chem. **13**(5), 436 (2023)
33. Wang, C.Y.: Free convection on a vertical stretching surface. J. Appl. Math. Mech. (ZAMM) **69**, 418–420 (1989)
34. Gorla, R.S.R., Sidawi, I.: Free convection on a vertical stretching surface with suction and blowing. Appl. Sci. Res. **52**, 247–257 (1994)
35. Devi, S.S.U., Devi, S.P.A.: Heat transfer enhancement of Cu-Al2O3 /water hybrid nanofluid flow over a stretching sheet. J. Nigerian Mathem. Soc. **36**, 419–433 (2017)
36. Ramya, D., Raju, R.S., Rao, J.A., Chamkha, A.: Effects of velocity and thermal wall slip on magnetohydrodynamics (MHD) boundary layer viscous flow and heat transfer of a nanofluid over a non-linearly-stretching sheet: a numerical study. Propuls. Power Res. **7**(2), 182–195 (2018)
37. Khan, A.U., Nadeem, S., Hussain, S.T.: Phase flow study of MHD nanofluid with slip effects on oscillatory oblique stagnation point flow in view of inclined magnetic field. J. Mol. Liq. **224**, 1210–1219 (2016)
38. Brewster, M.Q.: Thermal radiative transfer properties. John Wiley and Sons, New York (1972)
39. Sparrow, E.M., Cess, R.D.: Radiation heat transfer. Hemisphere, Washington (1978)
40. Raptis, A.: Radiation and free convection flow through a porous medium. Int Commun. Heat Mass Transf. **25**, 289–295 (1998)
41. Cebeci, T., Bradshaw, P.: Physical and Computational Aspects of Convective Heat Transfer. Springer, New York (1998)

42. Anwar, M.I., Shafie, S., Hayat, T., Shehzad, S.A., Salleh, M.Z.: Numerical study for MHD stagnation-point flow of a micropolar nanofluid towards a stretching sheet. J. Braz. Soc. Mech. Sci. Eng. **39**, 89–100 (2017)